Mathematical Modelling of Heat Transfer of Welding Arc (Part 1)†

Masao USHIO* and Fukuhisa MATSUDA**

Abstract

A mathematical formulation has been developed to represent the electromagnetic force field, the velocity field and the temperature field in DC welding arc. The formulation utilzed an engineering approach in which the plasma was regarded as a continuum of known electrical properties, the behavior of which could be represented by using the MHD equations and the convective heat balance relationships including the concept of turbulent nature of flow.

The calculations proceeded by specifying the arc dimensions and the arc current and then governning equations were solved numerically, ultimately yielding information on the velocity profiles and the temperature profiles within the system under the various conditions of electrode shapes.

The theoretical predictions of the temperature field and heat transfer characteristics are compared and discussed with experimental results.

KEY WORDS: (Arc Welding) (GTA welding) (Transport Phenomena Heat transfer) (Transport theory) (Arc simulation)

1. Introduction

In the welding arc such as gas-tungsten-arc and gas-metal-arc, a strong convective flow is induced along arc column. This self-generated convective flow plays some fundamental roles in the heat transfer on the work piece, the detachment and transfer of molten droplet from consumable electrode, the depression of surface of molten pool and many other physical phenomena during welding. The purpose of the work in this paper is to develop a mathematical modelling to describe quantitatively the velocity field, the temperature field and the heat transfer rates in atmospheric welding arc.

Maecker first explained[1] the generation of plasma flow in high current free-burning arc by the electromagnetically driven plasma which occur owing to the spatial non-uniformity of the current near the cathode. The current density is relatively high at the surface and in the vicinity of the cathode and gradually decrease toward the anode. This gradual increase of the current conducting cross-section from cathode to anode causes the axial pressure gradient and drives a flow of gas along arc column. And gas is drawn from surroundings into the arc column to maintain mass continuity. Experimental studies by Wienecke[2] and Bowman[3] show that the plasma velocity as high as 300 m/sec in a 200 A arc and 1500 m/sec in a 2.16 kA arc are reached.

In welding, the arc discharges between the rod electrode and the plate work piece in most cases. Though the rod electrode is not always the cathode, the current conducting cross-section expands from rod electrode toward plate electrode, then the coupled generation of gas flow take place similarly to the case of rod cathode.

In more recent years various refinement have been proposed, regarding Maecker's treatment, but because of simplifying assumptions the results have not been very satisfactory, either from the standpoint of providing reliable predictions or in giving a greatly improved insight into the behavior of these systems. Particularly in welding arc, the details of velocity, temperature fields and heat transfer to the plate under the various conditions of welding are little known, except the very simplfied analysis by Schoeck[4], Eckert and Pfender[5], and Quigley[6].

In a previous paper, Ushio, Szekely and Chang developed[7] the formulation for the high intensity air arc. Present work is not only the extension of above formulation to the case of welding arc, but also is based on the more appropriate assumption.

The motivation for the work to be described in the present work is the need to understand the transport phenomena of GTA welding and GMA welding on the basis of welding physics. The approach to be taken, will be to make use of recent development in the computation of MHD type flows. A complete solution of plasma state including atomic collision process is very difficult especially in the vicinity of interface between plasma and electrode. Therefore a little amount empirical input are still required in the present work, but it is thought to represent a major advance over prior work in this field.

† Received on March 31, 1982.

* Associate Professor

** Professor

Transactions of JWRI is published by Welding Research Institute of Osaka University, Ibaraki, Osaka, Japan

Regarding the organization of the papers, Part 1 is devoted to the formulation and computation on the influence of the shape of the cathode in the case of GTA welding, while the case of GMA welding is given in Part 2.

2. Formulation

In **Fig. 1** the physical situation and coordinate system are shown. A stationary axi-symmetric DC arc is applied between a rod electrode (cathode) and a plate (anode). Also shown in the figure are the r-z cylindrical coordinate system and the spatially variable arc radius.

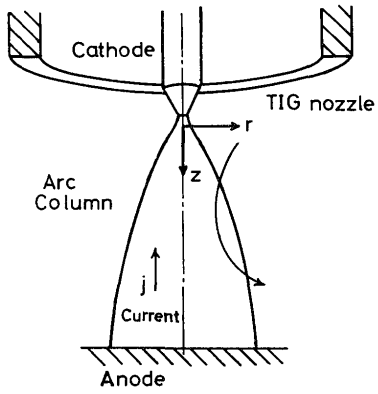

Fig. 1 Schematic drawing of TIG arc model and coordinate system.

The temperature are specified at the cathode and at the anode surface (shown in figures appeared in following section), furthermore we shall assume that the spatial distribution of the current is known.

If the nature of the fluid flow is turbulent or not depends on the profile of the force field, so we have to develop a statement of the electromagnetically driven fluid flow phenomena including the turbulent properties and the coupled heat transfer phenomena in the arc region.

The following principal assumptions are made;

1) The spatial distibution of the current and the electric field strength in the arc are known.
2) The driving force of the flow is only the electromagnetic forces thus the effect of buoyancy is neglected.
   The electromagnetic force can be calculated from Maxwell's equations.
3) The fuid is considered to be imcompressible and the turbulent fluid flow field could be represented in terms of the K-ε model for the turbulent viscosity.
4) Radiative transfer is neglected within the plasma, however an allowance is made for the spatially variable radiative heat loss from the plasma to the surroundings depending on the plasma temperature.
5) Some additional assumptions have been made in specifying the boundary conditions and these will be discussed subsequently.

The assumption that the spatial distribution of the current has to be known is thought to be the major weakness of the model, requiring empirical input information. However, according to the present knowledge[8], phenomena occuring in the zones adjacent to the electrodes are extremely complicated. Particularly in cathode region, strong contraction of the current and high field intensity make the thermal condition far from the equilibrium state and cause localized concentration of high energy density. For that reason the physical mechanism of cathode region is by no means as clearly understood yet. To make the problem manageable the distribution of the current and the electric field are both initially given using previous experimental works. This assumption, however, will have to provide an important link between the experimental and the theoretical work in this area.

As shown by Schoeck, the flow velocity of the order of 10^2 m/sec will result in the Mach number between 0.1–0.2. This gives a verification for the treatment that the fluid can be imcompressible.

The neglect of radiative heat transfer within the plasma is an oversimplification, which may be partially justified by the relatively small physical size considered, and by the absence of information of the radiative properties of the system such as welding arc including the impurity atom at relatively high level.

2.1 Governing equations

Within the framework of above assumptions the governing equations take the following form:

$$\nabla\cdot(\rho V)=0, \tag{1}$$
(equation of continuity)

$$\rho(V\cdot\nabla)V=-\nabla P-\nabla\tau+F, \tag{2}$$
(equation of motion)

$$\rho(V\cdot\nabla h)=\nabla\cdot\kappa_{\mathrm{eff}}\nabla T+S_{\mathrm{T}}, \tag{3}$$
(thermal energy balance equation)

where, ρ : mass density,
V : velocity vector,

If J(r,z) is given we may evaluate **B**(r,z) and hence **F**(r,z) from Maxwell's equations.

∇P: pressure gradient,
τ : stress tensor, which includes both laminar and turbulent stresses,
F : body force vector, which represents elctromagnetic force field, $F=J\times B$,
κ_{eff} : effective thermal conductivity,
J : current density vector,
B : magnetic flux vector,
S_T : source term which represents the Joule heat generation and radiation loss,
h : enthalpy.

In order to determine the flow field and transport phenomena, it is necessary to solve simultaneously some additional equations which describe electromagnetic field, relationship between material variables and turbulent properties and boundary conditions.

Upon defining the vorticity and the stream function the axi-symmetric form of the equation of motion takes the following form (ξ: vorticity, ψ: stream function),

$$\frac{\partial}{\partial z}\left(\frac{\xi}{r}\frac{\partial\psi}{\partial r}\right)-\frac{\partial}{\partial r}\left(\frac{\xi}{r}\frac{\partial\psi}{\partial z}\right)-\frac{\partial}{\partial z}\left\{\frac{\mu_{eff}}{r}\frac{\partial}{\partial z}(r\xi)\right\}-\frac{\partial}{\partial r}\left\{\frac{\mu_{eff}}{r}\frac{\partial}{\partial r}(r\xi)\right\}-\left(\frac{\partial F_r}{\partial z}-\frac{\partial F_z}{\partial r}\right)=0, \quad (4)$$

$$\frac{\partial}{\partial z}\left(\frac{1}{\rho r}\frac{\partial\psi}{\partial z}\right)+\frac{\partial}{\partial r}\left(\frac{1}{\rho r}\frac{\partial\psi}{\partial r}\right)+\xi=0, \quad (5)$$

where, μ_{eff} the effective viscosity is defined as

$$\mu_{eff}=\mu_l+\mu_t. \quad (6)$$

μ_t the turbulent viscosity has been represented in terms of the K-ε model.[9]

$$\mu_t=C_D\rho\kappa^2/\varepsilon, \quad (7)$$

C_D : dissipation constant,
K : turbulence kinetic energy per unit mass,
ε : dissipation rate of turbulence energy.

Of cource we might be able to neglect the turbulent nature of flow in the case of low current GTA welding, but in the case, we can substitute zero for the turbulent viscosity. K and ε are determined by solving the following conservation equations:

$$\frac{\partial}{\partial z}\left(K\frac{\partial\psi}{\partial r}\right)-\frac{\partial}{\partial r}\left(K\frac{\partial\psi}{\partial z}\right)-\frac{\partial}{\partial z}\left\{r\frac{\mu_{eff}}{\sigma_k}\frac{\partial K}{\partial z}\right\}-\frac{\partial}{\partial r}\left\{r\frac{\mu_{eff}}{\sigma_k}\frac{\partial K}{\partial r}\right\}-rS_k=0, \quad (8)$$

$$\frac{\partial}{\partial z}\left(\varepsilon\frac{\partial\psi}{\partial r}\right)-\frac{\partial}{\partial r}\left(\varepsilon\frac{\partial\psi}{\partial z}\right)-\frac{\partial}{\partial z}\left\{r\frac{\mu_{eff}}{\sigma_\varepsilon}\frac{\partial\varepsilon}{\partial z}\right\}-\frac{\partial}{\partial r}\left\{r\frac{\mu_{eff}}{\sigma_\varepsilon}\frac{\partial\varepsilon}{\partial r}\right\}-rS_\varepsilon=0, \quad (9)$$

the source terms S_k and S_ε are defined as:

$$S_k=2\mu_t\left\{\left(\frac{\partial V_z}{\partial z}\right)^2+\left(\frac{\partial V_r}{\partial r}\right)^2+\left(\frac{V_r}{r}\right)^2+\frac{1}{2}\left(\frac{\partial V_r}{\partial z}+\frac{\partial V_z}{\partial r}\right)^2\right\}-\rho\varepsilon, \quad (10)$$

$$S_\varepsilon=2C_1\mu_t\frac{\varepsilon}{K}\left\{\left(\frac{\partial V_z}{\partial z}\right)^2+\left(\frac{\partial V_r}{\partial r}\right)^2+\left(\frac{V_r}{r}\right)^2+\frac{1}{2}\left(\frac{\partial V_r}{\partial z}+\frac{\partial V_z}{\partial r}\right)^2\right\}-C_2\rho\frac{\varepsilon^2}{K}. \quad (11)$$

Here, σ_k and σ_ε are effective Prandtl number for transport of K and ε respectively. C_1, C_2 and C_D are constants and the values of these constants are listed in **Table 1**.

Heat transport equation is

$$C_P\frac{\partial}{\partial z}\left(T\frac{\partial\psi}{\partial r}\right)-C_P\frac{\partial}{\partial r}\left(T\frac{\partial\psi}{\partial z}\right)-\frac{\partial}{\partial z}\left\{rC_P\frac{\mu_{eff}}{\sigma_T}\frac{\partial T}{\partial z}\right\}-\frac{\partial}{\partial r}\left\{rC_P\frac{\mu_{eff}}{\sigma_T}\frac{\partial T}{\partial r}\right\}-rS_T=0, \quad (12)$$

where, Prandtl number $\sigma_T=\dfrac{C_P\mu_{eff}}{\kappa_{eff}}$.

S_T represents source term, which contains the Joule heat generation and the radiation loss,

$$S_T=J\cdot E-S_R. \quad (13)$$

Radiative transport is known to be an important energy transfer mechanism in high temperature electric arcs. Radiation losses generally have to be calculated as a function of wave length, generally extending into the far ultraviolet region of the spectrum. But, in view of the complexity of the evaluation of spectral intensity owing to the existence of some impurity atom, a semi-empirical form is boldly used[10].

Table 1 Numerical values of parameters and constants

C_D	dissipation constant	0.09
C_1	constant of K-ε model	1.44
C_2	constant of K-ε model	1.92
σ_K	Prandtl number for K	1.0
σ_ε	Prandtl number for ε	1.3
σ_T	Turbulent prandtl number	0.9
ρ	Mass density	0.05 kg/m^3
C_P	Specific heat	3100 J/kg °K
T_w	temperature at anode	2500°K
EB	arc length	10 mm
R(0)	arc radius at cathode	0.45 mm
R(z)	arc radius at anode	1.7 mm
I_t	total discharge current	200 A
V_A	arc voltage	13 V
	Gas flow rate (Argon)	10 l/min

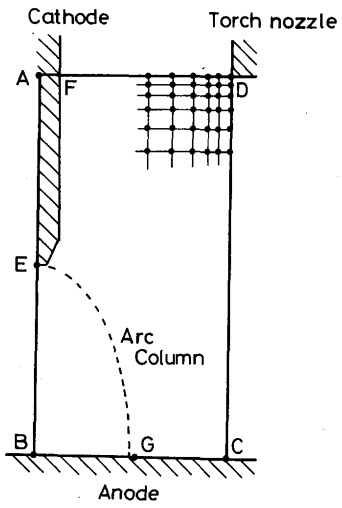

Fig. 2 Domain and boundaries to be solved and a part of grid nodes.

$$S_R \propto \frac{1}{T} \exp(-eV_i/kT), \tag{14}$$

where, V_i: effective ionization potential of working gas,

k : Boltzman constant.

The value of the constant of proportionality was deduced data reported by Evans and Tankin.[11]

2.2 The boundary conditions

The physical domains over which the boundary conditions are specified are skeched in **Fig. 2.**

In a physical sense the boundary conditions will specify:

1) The velocity field at the outlet of the shield nozzle.
2) The temperature at the cathode surface.
3) The temperature at the anode.
4) No slip condition at the anode and cathode surfaces and symmetry about the central axis of a the arc column.

The actual velocity distribution at $z=0$ may be estimated from pipe flow data:

$$v_z = \frac{2Q}{\pi\rho}\left[R_2^2 - r^2 + \frac{(R_2^2-R_1^2)\ln\left(\frac{r}{R_2}\right)}{\ln(R_2/R_1)}\right] \Big/ \left[R_2^4 - R_1^4 - \frac{(R_2^2-R_1^2)^2}{\ln(R_2/R_1)}\right] \tag{15}$$

where, Q: flow rate, R_2=AD, R_1=AF.

In the $z=0$ plane the remaining boudary conditions take the following form:

$$\xi = \frac{\partial\psi}{\partial z} = K = \varepsilon = \frac{\partial T}{\partial z} = 0. \tag{16}$$

Current density distribution is assumed to be parabolic one:

$$J = J_0\left\{1 - \left(\frac{r}{R}\right)^2\right\}, \quad (R=R(z)\text{: arc radius}). \tag{17}$$

At the cathode surface, the temperature was distributed adequately in the range from 3000°K to 1000°K. Though the values of surface tempersture are the boundary values of the calculations, it is thought to give no decisive influence on the temperature profile of the arc region.

At the axis of symmetry, i.e. at $r=0$ we have,

$$\psi = \frac{\partial K}{\partial r} = \frac{\partial \varepsilon}{\partial r} = \frac{\partial T}{\partial r} = 0,$$

$$\left(\frac{\xi}{r}\right)_0 = \frac{8}{\rho}\left\{\frac{\psi_0-\psi_1}{r_2^2} + \frac{\psi_1-\psi_0}{r_1^2}\right\} \Big/ (r_2^2-r_1^2). \tag{18}$$

where, suffixes 0, 1 and 2 denote the points on the axis of symmetry and the adjacent grid nodes in the r-direction, respectively.

At the anode surface,

$$T = T_w. \tag{19}$$

Furthermore,

$$\psi = K = \varepsilon = 0, \tag{20}$$

and the following expression is applied to the vorticity,

$$\left(\frac{\xi}{r}\right)_0 = \frac{3(\psi_0-\psi_1)}{\rho r^2 (z_1-z_0)^2} - \frac{1}{2}\left(\frac{\xi}{r}\right)_1, \tag{21}$$

where, suffix 0 and 1 refer to a grid node of the boundary and the adjacent node in z-direction, respectively.

Finally at the surface CD, we have,

$$\frac{\partial\psi}{\partial r} = \frac{\partial\xi}{\partial r} = \frac{\partial K}{\partial r} = \frac{\partial\varepsilon}{\partial r} = \frac{\partial T}{\partial r} = 0. \tag{22}$$

It is known that the steep gradients of transport properties exist in the vicinity of the wall. In the immediate vicinity of the wall the fluid is in laminar motion and the effective viscosity and thermal conductivity are very much lower than they are at even a short distance from the wall. The behavior of the near wall region can be modelled by the use of wall function method[12]. In this study the wall function method is applied for the turbulence quantities (K and ε). Velocity distribution in the vicinity of the wall is expressed in terms of the "logarithmic law",

$$V_+ = \frac{1}{\beta}\ln(En_+), \tag{23}$$

where, β : von Karman's constant,
E : function of wall roughness approximately equal to 9 for a smooth wall,
V_+ : dimensionless velocity parallel to wall $=\frac{V_\tau}{V_\tau}$,
V : friction velocity $=\tau_w/(\rho C_D^{1/4} K^{1/2})$,
n : dimensionless distance from the wall $=\frac{nV_\tau}{\mu\tau_w}$,
n_+ : distance of the node from the wall.

If $n_+ \geqq 11.5$, τ_w can be evaluated by using the following relationship[17];

$$\tau_w=\beta C_D^{1/4}\rho V_{r_1} K_1^{1/2}/\ln[E\rho n_1 K_1^{1/2} C_D^{1/4}/\mu], \tag{24}$$

where, suffix 1 denotes the adjacent grid to the wall. The source term for the turbulence kinetic energy, S_k can be written as

$$S_k=\tau_w\frac{\partial V_r}{\partial n}-\frac{C_D\rho^2K^2}{\mu_t}, \tag{25}$$

and dissipation rate is

$$\varepsilon_1=C_D^{3/4}K_1^{3/2}/\beta n. \tag{26}$$

2.3 Heat transfer to the anode plate

The heat transfer phenomena in the welding arc is somewhat more complex than in conventional transport case, because in addition to convective heat transfer, thermal energy is also transfered to the plate by thermal radiation, and by the electron or ion, which penetrate the plate surface. In the GMA welding the heat transfer by the molten droplets is added, too.

Here we can show the case of the GTA welding. A schematic representation of thermal energy exchange between the anode plate and the arc plasma is illustrated in **Fig. 4**. The factors involved the figure are already referred by Schoeck, Eckert and Pfender, and Quigley. Therefore, some brief descriptions are given for the representations of these factors in the figure.

Q_A represents the sum of the directional kinetic energy of electrons accelerated by anode fall electric field and the potential energy given up by electrons on entering the anode corresponding to the work function of the anode metal[4,5,6]. Q_E is the electron thermal energy transported by Thomson effect. Q_R is the radiation energy transferred from the arc to the anode. Q_C is the heat input by conduction and convection. Q_v and Q_a represent the heat loss by evaporation and the heat radiated from the plate surface to the environment. In all these quantities, Q_E and Q_C are related with the computation of the arc flow field.

Q_E is described as follows;

$$Q_E=\frac{j}{e}\frac{3}{2}k(\alpha T_1-T_w), \tag{27}$$

where, j current density at the plate surface,
k Boltzman constant
T_e electron temperature at the adjacent node to the plate surface, which is assumed slightly high comparing the heavy particle temperature at the point T_1, then in the present work $\alpha(=T_e/T_1)$ was taken at 1.2,
e electron charge.

The expression for Q_c is introduced from the results of the reentry problem studies according to Eckert and Pfender[5,13,14]

$$Q_c=\frac{Nu}{Re^{1/2}Pr}\left\{\rho_w\mu_w\frac{dV_b}{dz}\right\}^{1/2}C_b(T_b-T_w), \tag{28}$$

$$\frac{Nu}{Re^{1/2}}=0.915\,Pr^{1/4}\left(\frac{\rho_e\mu_e}{\rho_w\mu_w}\right)^{0.43}, \tag{29}$$

where, Nu: Nusselt number,
Re : Reynolds number,
Pr : Prandtl number,
C_b : Specific heat.

Suffix, w and b denote the point on the wall surface

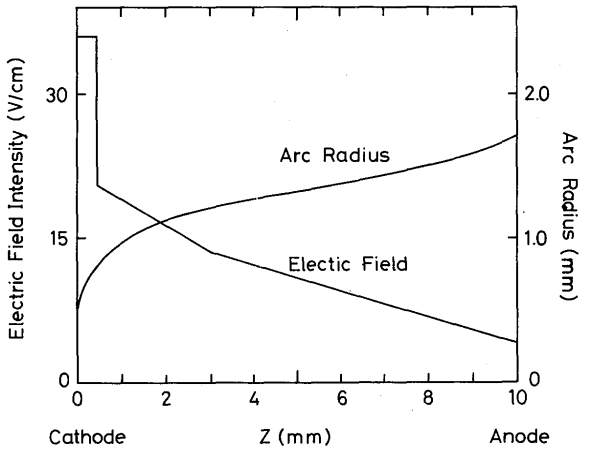

Fig. 3 Electric field distribution along z-axis and arc radius, which are intially given.

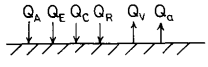

Fig. 4 Various heat transfer mechanisms to the anode.

and the edge of the boundary layer. In the calculation of eq. (12), heat flux through the anode plate is replaced by the sum of Q_E and Q_C.

3. Solution Procedure

The governing equations were put in dimensionless finite difference forms using 41×41 non uniform mesh grid according to the technique described by Gosman et al.[15], and solved numerically. Those equations were integrated over the area defined by the rectangle enclosing a grid point. In the vicinity of the wall, the diffusion of the turbulence kinetic energy through the wall was set equal to zero and the dissipation rate of turbulence energy near the wall is calculated by using the form given by Spalding[9].

Introducing the Gauss-Seidel method, point iteration process were made until the following convergence criterion could be satisfied in all variables.

$$\frac{\Sigma|\phi_j^{(N)}-\phi_j^{(N-1)}|}{\Sigma|\phi_j^{(N)}|} < \delta \qquad (30)$$

where, j denotes the species of variables, $\phi^{(N-1)}$ is the value of the variable calculated in the (N-1)th iteration and $\phi^{(N)}$ is the one calculated in the (N)th iteration. Σ means summation over all interior nodes. δ has been set in the range 0.001–0.003.

The computer time required was of the order of 200 sec in CPU time on the ACOS-900-system of Osaka University.

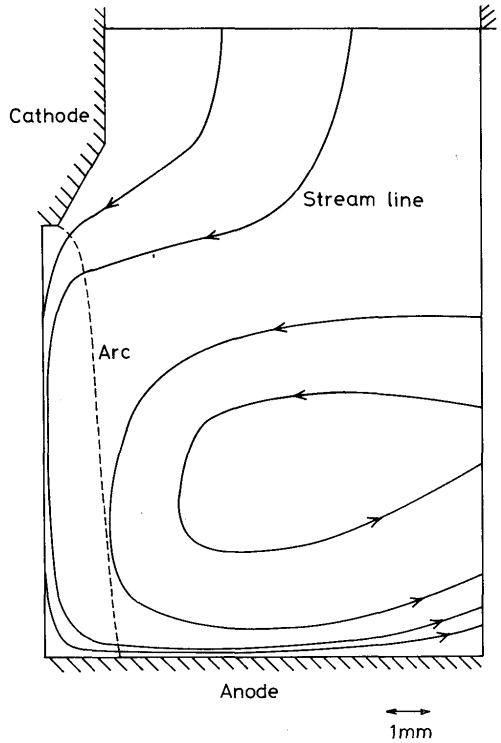

Fig. 5 Computed flow pattern under the condition of 200 A argon arc of 10 mm in length with type-A cathode.

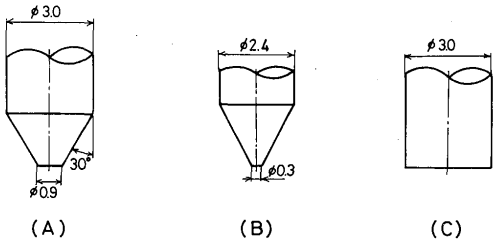

Fig. 6 Various types of cathode.

4. Results and Discussions

In the present paper, a major interest is to present the formulation for calculation of the velocity and temperature fields and the heat transfer rates and the some computed results about the above problems for the GTA welding arc.

The electrical conditions, the numerical parameters and constants are shown in **Fig. 3** and Table 1. The thermal properties of the working gas, argon, are assumed to be constant. In order to investigate the change in the velocity field owing to the sharpness of the cathode tip, three types of cathode are employed. Those are shown in **Fig. 6**.

Figure 5 shows the flow pattern of the fluid in the case of the type-A cathode. Stream lines which are constant-ψ lines represent the inhaling surrounding gas and the generating stagnation flow. It is noticed the recirculating flow can exist around the arc column. The scale length of this recirculating flow is thought to be related to the degree of completeness of shielding of the arc welding from the air, however we have not yet sufficient data to be shown.

The change in the flow velocity along the central axis is shown in **Fig. 7**. Plasma is accelerated to the maximum velocity of 210 m/sec in the region in less than 1 mm in distance from the cathode. In turbulence energy map two peaks existed, which are the one in the neighbourhood of cathode region and the other just above the stagnation zone. In those domains, the values of μ_t/μ_{eff} are around 0.3, relatively high, while at the side of the cathode the value is 0.03. The flow has slightly the turbulent nature but the turbulent region is very narrow. The upper peak of turbulence energy is responsible to the decay of axial velocity in upstream region and is due to the enhanced non-uniformity in velocity field by strong extension of current path in this region.

The force field derived from the assumed current distribution is shown in **Fig. 8**. The distribution of radial and axial components of the body force along

the arc column at the radial position of $r=0.15$ mm are given in the figure. In the neighbourhood of the cathode, the current conducting cross-section has a large widening, so that the value of F_z is comparatively high than those in the cental region of the gap between two electrodes. F_z gives the strongly decaying curve toward the anode, while F_r is gradually changed. This means the major character of the flow may be determined by the change in current conducting cross-section in the neighbourhood of the cathode tip. It should be remarked that the computed results are found to be quite sensitive to the arc radius assumed, particularly to the one near the cathode. Another factor influencing on the velocity profile and turbulent nature without current profile will shown later.

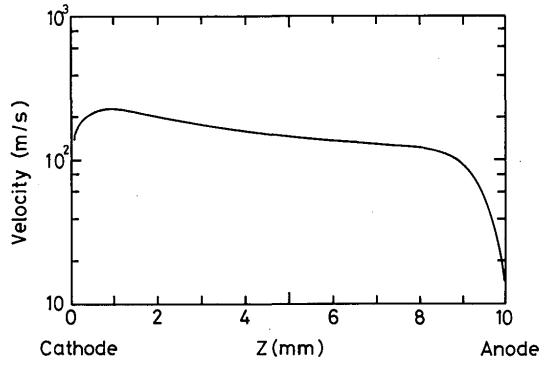

Fig. 7 Computed axial velocity distribution on the ceter line with type-A cathode.

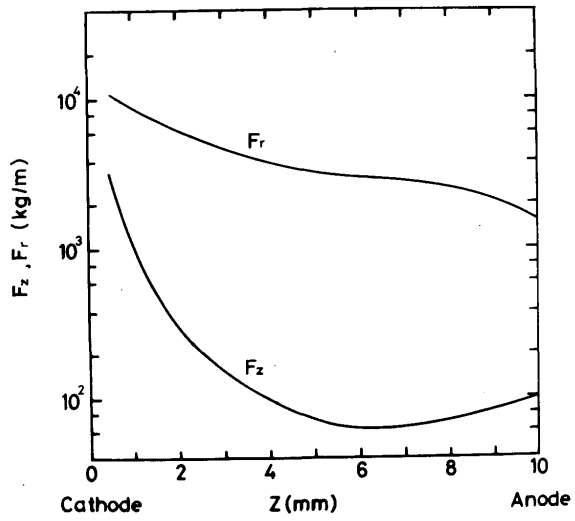

Fig. 8 Radial and axial components of body force vector along arc column at the radial position of r=0.15 mm.

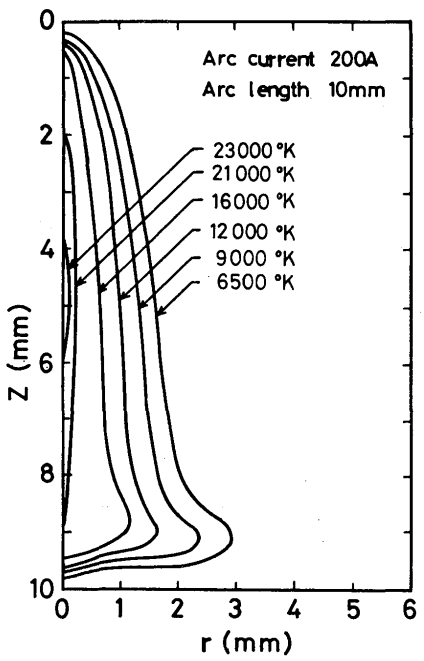

Fig. 9 Computed temperature profile of the arc in the case of type-A cathode.

The temperature profile of the arc is shown in **Fig. 9**. The well-known bell-shaped contour of arc can be seen in some isotherm line. As a matter of cource these isotherm contour do not coinside with the stream line.

The maximum temperature region exists in the central part of the arc in contrast with the many experimental results[6,10,16]. This might be, also, due to the slenderness of arc profile, the unappropriateness of electric field distribution and the oversimplification of material constants of working gas, assumed.

The electric field intensity is relatively high in the neighbourhood of the cathode tip. The thickness of cathode fall region is much less than this high intensity field thickness shown in Fig. 3. The cathode fall is widely understood to have the electric field of the order of 10^4 V/cm, while the thickness of some 10^{-4} cm. The heat generation at and in the vicinity of the cathode fall region has a strong influence on temperature profile of the arc, but it occurs in the much narrower area than the size of mesh to be used for the calculation. So, in order to reflect this heat generation to the temperature profile through calculation by using the more rougher mesh, relatively high electric field is assumed at the adjacent node to the cathode surface. The overall distribution of the electric field is determined so that the voltage drop along arc column is to be 11 V and the anode fall voltage is 2 V. This high intesity field has a effect only on the heat generation, therefore, more reasonable temperature

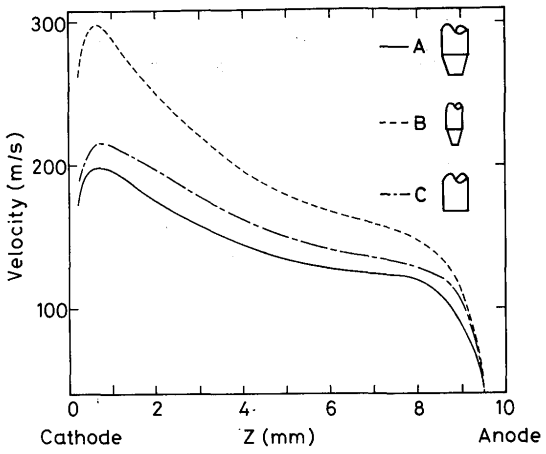

Fig. 10 Change in velocity distribution on the central axis with various shapes of cathode tips under the same condition of arc profile.

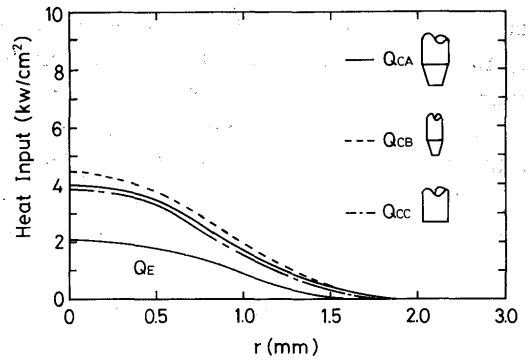

Fig. 11 Comparison of heat inputs in cases of various electrodes.

profile could be obtain by using the more fine mesh in the neighbourhood of the cathode.

The change in velocity distribution along arc column due to the variation in shape of the cathode tip are studied by using the three types of electrode under the same condition about the arc profile. The results are shown in **Fig. 10**. This results mean the shape of the cathode tip also gives the influence on the velocity of induced flow without the current distribution. Type-C cathode has the highest impedance for the induced flow in the three cathodes. These results are qualitatively agreed with experimental results on pressure measurement by Schoeck[4] and Petrie and Pfender[16]. The maximum velocity is obtained with type-B cathode, which is around 300 m/sec. Additionally in this case the turbulence energy is least among the three cases.

Figure 11 shows the spatial distribution of heat fluxes falling on the anode surface, due to the various mechanism of heat transfer. Here Q_c is combined convective and conductive heat flux, Q_E is the heat flux due to the Thomson effect. Three types of cathode have some difference in Q_c in accordance with those in velocities. Integrated heat inputs of Q_c and Q_E are respectively around 8% and 5% of the total arc power. These values are in good agreement with Quigley's estimation about the heat balance of argon welding arc. The contribution of the convective and conductive heat transfer to the total heat input to the anode are very low compared with the one due to the anode fall or anode work function. But in the case of high current, the heat input by the convection and conduction increase significantly. The situation might be realized in the high current GMA welding.

5. Conclusions

In the paper a mathematical formulation has been developed to represent the elecromagnetic force field, the velocity field and the temperature field in DC welding arcs.

In essence the formulation utilzed an engineering approach, in which the plasma was regarded as a continuum, of known electrical properties, the behavior of which could be represented by using the turbulent MHD equation and the turbulent convective heat balance relationships.

The calculation proceeded by specifying the arc dimension and the arc current and electric field distributions, and then the governing equations were solved numerically, ultimately yielding information on the velocity profiles, the temperature profiles and on the heat transfer rates to the anode surface.

The computed results for the velocity field of GTA welding arc has provided some interesting features on the fluid flow phenomena of welding arc, i.e. the recirculating flow in the shielding gas and the factors influencing the efficiency of heat transfer. Notwithstanding the major simplifying assumptions that have been made, particularly the need for empirical input regarding the current distribution and the arc radius, it is suggested that the present fromulation could provide an understanding the transport phenomena in welding arcs.

Additionally the calculations presented here afford the following conclusions. The shape of the cathode tip has an influence on the velocity of self-induced flow of arc. The higher velocity around 300 m/sec was obtained with tapered cathode tip in the neighbourhood of the cathode surface under the condition of 200 A argon arc of 10 mm in length.

Furthermore, the sharpness of the cathode tip increases the heat transfer efficiency due to convective and conductive mechanism through the increase of axial velocity of induced flow.

Acknowledgement

The authors wish to thank Mr. K. Takase, formerly student for his valuable contributions to the work.

Referensecs

1) H. Maecker; Z. Physics vol. 141, pp 198, 1955.
2) R. Wienecke; Z. Physics vol. 143, pp 128, 1955.
3) B. Bowman; J. Phys. D. Appl. Phys. vol. 5, pp 1422, 1972.
4) P.A. Schoeck; in "Modern Development in Heat Transfer", pp 353, Academic Press, N.Y. 1963.
5) E.R.G. Eckert and E. Pfender; in "Advances in Heat Transfer vol. 4", pp 229, Academic Press, N.Y., 1967.
6) M.B.C. Quigley, P.H. Richards, D.T. Swift-Hook and A.E.F. Gick; J. Phys. D. Appl. Phys. vol. 6., pp 2250, 1973.
7) M. Ushio, J. Szekely and C.W. Chang; Iron making and Steel Making vol. 8, pp 279, 1981.
8) G. Ecker; IEEE Trans. Plasma Sci. PS-4, pp 218, 1976.
9) B.E. Launder and D.B. Spalding; Comp. Methods in Appl. and Engr. vol. 3, pp 269, 1974.
10) H. Edels; Inst. Electr. Engr., pp 55, 1963.
11) D.L. Evans and R.S. Tankin; Phys. Fluids vol 10, pp 1137, 1967.
12) H. Schlichting; "Boundary Layer Theory", McGraw-Hill, 1968.
13) J.P. Hartnett; Mass transfer Cooling, in Handbook of Heat Transfer, McGraw-Hill, 1973.
14) A. Pallone and W.V. Tassel; Phys. Fluids vol. 6, pp 983, 1963.
15) A.D. Gosman, W.M. Pun, A.K. Runchal, D.B. Spalding and M. Wolfstein; "Heat and Mass Transfer in Recirculating Flows", Acedemic Press, 1969.
16) T.W. Petrie and E. Pfender; Welding Journal, pp 588s, 1970.
17) W.M. Pun and D.B. Spalding; "A General Computer Program for Two-Dimensional Elliptic Flows", Report HTS/76/2, Heat Transfer Section, Imperial College of Science and Technology (1976).

Nomenclature

$\boldsymbol{B}$; Magnetic flux density vector
C_p ; Specific heat
C_1, C_2, C_D ; Constants of K-ε model of turbulence and dissipation constant
e ; Electron charge
$\boldsymbol{E}$; Electric field vector
$\boldsymbol{F}, \boldsymbol{F}_r, \boldsymbol{F}_z$; Body force vector and its radial and axial components
h ; Enthalpy
$\boldsymbol{J}, \boldsymbol{J}_0$; Current density and its value at r=0
k ; Boltzman constant
K ; Turbulent kinetic energy
n_+, n_τ ; distance of the node from the wall and its dimensionless value
P ; Pressure
Q_A, Q_E ; Energy flux caused by anode fall and anode work function and by Thomson effect
Q_c, Q_R, Q_V, Q_a ; Energy flux by conduction and convection, by radiation from arc, by vaporization from the anode and by radiation from the anode
r ; Radial coordinate
S_K, S_ε ; Source terms for K and ε transport equation and radiation loss term
T, T_0, T_w, T_e ; Temperature, and its value at z=0, at the anode wall surface and the electron temperature in the vicinity of the anode
V, v_r, v_z, v_0 ; Velocity vector and its radial and axial components, and its value at the edge of the boundary layer
V_τ, V_+ ; Friction velocity and dimensionless velocity parallel to the wall
V_i ; Effective ionization potential of the working gas
z ; Axial coordinate
α ; Ratio between electron and heavy particle temperature in the vicinity of anode
β ; Von Karman's constant
δ ; Convergence criterion
ε ; Dissipation rate of turbulence energy
κ, κ_{eff} ; Thermal conductivity and its effective value
μ_l, μ_t, μ_{eff} ; Laminar, turbulent and effective viscosity
ξ ; Vorticity
ρ ; Mass density
$\sigma_K, \sigma_\varepsilon, \sigma_T$; Prandtl number for K, ε and turbulent Prandtl number
ψ ; Stream function'
τ, τ_w ; Stress tensor and its value in the vicinity of anodewall